Theoretical and laboratory study of suppression effects in fine-structure-changing collisions of Ti with He

Bernard Zygelman*
Department of Physics and Astronomy, University of Nevada Las Vegas, Las Vegas, Nevada 89154, USA

Jonathan D. Weinstein
Department of Physics, University of Nevada, Reno, Nevada 89557, USA

(Received 14 March 2008; revised manuscript received 7 June 2008; published 18 July 2008)

We report on the results of a multichannel calculation of fine-structure transition cross sections for collisions of ground-state Ti with He. We find significant suppression of fine-structure level quenching over a wide range of collision energies. We show that the suppression is due to a mechanism proposed by [Hancox *et al.*, Nature (London) **431**, 281 (2004)] to explain similar suppression of Zeeman relaxation in collisions of magnetically trapped rare-earth-metal atoms with cold He atoms. We find that the quenching rates are sensitive to the value of the Born-Oppenheimer adiabatic potential surfaces of the Ti-He system in the region of the inner repulsive wall. Adjusting the *ab initio* potentials for TiHe, available in the literature, we find good agreement with laboratory measurements.

DOI: 10.1103/PhysRevA.78.012705 PACS number(s): 34.50.Cx, 34.20.-b

I. INTRODUCTION

Fine-structure-changing collisions control the cooling of interstellar clouds [1] and the heat budget of planetary atmospheres [2,3], allow for diagnostic probes of laboratory and astronomical plasmas [4] and, therefore, have been the topic of numerous theoretical and laboratory investigations [5–9]. In the past decade, attention in the atomic collision community has shifted to understanding and controlling cold and ultracold matter. The advances that led to the first laboratory demonstrations of Bose Einstein condensation (BEC) in atomic vapors were confined to species in which the interatomic interaction is largely isotropic. The recent focus is on species that involve intrinsic, internal, orbital angular momentum, which leads to anisotropic interactions among the collision partners [10–12]. Collisions involving atoms and molecules that have nonzero internal orbital angular momentum are expected to exhibit large inelastic cross sections that can lead to the loss of the atoms in a magnetic trap[12,13]. Doyle and co-workers [13] suggested the use of rare-earth-metal atoms to address the problem of Zeeman relaxation and trap loss due to anisotropic interactions with the buffer gas. They argued that, in the rare-earth metals, angular coupling effects may be suppressed due to the screening of the open *d*-shell electrons by the closed outer *s*-shell electrons. Detailed calculations [14–16] and laboratory measurements [13] of *m*-changing collisions of rare-earth-metal atoms with He have validated the general conclusion of that thesis.

In this study we consider the fine structure (FS) relaxation of titanium with a He buffer gas. Because FS transitions are also driven by anisotropic interactions [17], one expects a similar suppression. Here we undertake a study of fine-structure relaxation in the Ti-He system that spans a collision energy range from cold to superthermal. At higher energies many partial waves participate in the collision, and anisotropy effects become increasingly important. Previous work focused on systems involving a strong magnetic field, but we consider the zero-field limit where the Zeeman levels are degenerate. Our choice to study the Ti-He system is several-fold. Cold He is the buffer gas of preference in trapping experiments [18], the Ti-He system was studied in the Zeeman-relaxation experiments of Doyle, and laboratory measurements of FS relaxation in this system have recently become available [19]. The results of our calculations add to the collision database for Ti, which has many applications including its use as a dopant in hydrogen-storage applications [20].

In Sec. I we briefly summarize the multichannel theory used in these calculations. A more detailed discussion of the underlying theory has been given in Ref. [17]. Our results are presented in Sec. II, and they suggest that the screening mechanism of Doyle is also responsible for the suppression of FS transitions over a wide collision energy range. At higher collision energies, in the thermal to superthermal range, suppression may be less effective since the system samples regions where the He atom has significant overlap with the electron cloud of the Ti atom. We introduce a small modification of the *ab initio*, ground, Born-Oppenheimer (BO) potentials for the TiHe molecule in order to bring the results of the calculations into agreement with our laboratory measurements. Our calculations suggest that a more accurate description of the BO curves, in the region of the inner repulsive wall, is required in order to make definitive predictions for cross sections at thermal and higher collision energies. In the Appendix we briefly compare the theory presented here with those used in previous calculations for *m*-changing transitions. Atomic units are used throughout, unless otherwise stated.

II. THEORY

We apply a theory of fine-structure excitation of complex atoms that was introduced in Ref. [17], and employed in [21]

*bernard@physics.unlv.edu

to estimate collisional fine-structure excitation rate coefficients for two oxygen atoms in their ^3P_J manifold. Here we consider the special case where one atom is a closed S-shell system. We seek solutions to the multichannel scattering amplitudes $F_{j\Omega}(\boldsymbol{R})$, where the channel indices $j\Omega$ are the total and azimuthal electronic angular momentum quantum numbers for the TiHe diatom. They satisfy the Schrödinger equation

$$\nabla^2 F_{j\Omega}(\boldsymbol{R}) - 2\mu \sum_{j'\Omega'} V_{j\Omega}^{j'\Omega'}(R,\theta,\phi) F_{j'\Omega'}(\boldsymbol{R}) + k_j^2 F_{j\Omega}(\boldsymbol{R}) = 0, \tag{1}$$

where μ is the reduced mass of the Ti-He system, k_j^2 is the wave number for channel $j\Omega$ which depends on the FS energy defects of the TI atom, and $V_{j\Omega}^{j'\Omega'}(R,\theta,\phi) \equiv \underline{V}(R,\theta,\phi)$ is a multichannel potential discussed below. We ignore nonadiabatic couplings, which are expected to be small [17].

For two atoms a and b with total electronic angular momenta j_a and j_b, respectively, the anisotropic interatom potential is given by [17]

$$\begin{aligned} V(R,\theta,\phi) = & \sum_{\Lambda\Sigma} \sum_{LS} [j,j',j_a,j_b,j_a',j_b']^{1/2}[L,S] \\ & \times \sum_{\Omega_1} D^{j}_{\Omega,\Omega_1}(\phi,\theta,-\phi) D^{j'}_{\Omega_1,\Omega'}(\phi,-\theta,-\phi) \\ & \times \begin{pmatrix} L & S & j \\ \Lambda & \Sigma & -\Omega_1 \end{pmatrix} \begin{pmatrix} L & S & j' \\ \Lambda & \Sigma & -\Omega_1 \end{pmatrix} \\ & \times \begin{Bmatrix} l_a & s_a & j_a \\ l_b & s_b & j_b \\ L & S & j \end{Bmatrix} \begin{Bmatrix} l_a' & s_a' & j_a' \\ l_b' & s_b' & j_b' \\ L & S & j' \end{Bmatrix} \epsilon_{\Lambda S L}(R) \end{aligned} \tag{2}$$

where

$$D^{j}_{\Omega,\Omega'}(\phi,\theta,-\phi) \equiv \langle j\Omega | \exp(-i\phi j_z)\exp(-i\theta j_y)\exp(i\phi j_z) | j\Omega' \rangle \tag{3}$$

is a Wigner rotation matrix, L and S are the total electronic orbital and spin angular momenta of the system, l_a, l_b and s_a, s_b are the individual atomic orbital and spin angular quantum numbers, respectively, j, j' are the total diatomic electronic angular momenta, and $\epsilon_{\Lambda S L}(R)$ are the Born-Oppenheimer eigenenergies for the molecular system formed in the approach of the two atoms. Equation (2) is applicable if we can make a one-to-one correspondence between the asymptotic state quantum numbers and the quantum numbers that itemize the Born-Oppenheimer states [17]. Such was the case considered in Ref. [21], that of two atoms in the $^{(2S+1)}P_J$ manifold. It also applies to the case considered here, one atom in an $l_a=0, s_a=0, j_a=0$ state (the He atom) and the other in $j=j_b=4,3,2$ states (the Ti atom). Inserting these quantum numbers into Eq. (2) we arrive at the simplified expression

$$\begin{aligned} V(R,\theta,\phi) = & \sum_{\Omega_1} [j,j']^{1/2} \mathcal{D}^{j}_{\Omega\Omega_1}(\phi,\theta,-\phi) \mathcal{D}^{j'}_{\Omega_1\Omega'}(\phi,-\theta,-\phi) \\ & \times \sum_{\Lambda M_S} \begin{pmatrix} L & S & j \\ \Lambda & M_S & -\Omega_1 \end{pmatrix} \begin{pmatrix} L & S & j' \\ \Lambda & M_S & -\Omega_1 \end{pmatrix} \epsilon_\Lambda(R), \end{aligned} \tag{4}$$

where $L=l_b=3$, $S=s_b=1$, and we itemized the BO potentials $\epsilon_\Lambda(R)$ solely in terms of the projection of the orbital electronic angular momentum on the internuclear axis. In deriving Eq. (4) we made use of the fact that

$$\begin{Bmatrix} 0 & 0 & 0 \\ l_b & s_b & j_b \\ L & S & j \end{Bmatrix} = \frac{\delta_{L,l_b}\delta_{S,s_b}\delta_{j,j_b}}{[j,L,S]^{1/2}}. \tag{5}$$

To gain a better understanding of the mechanism that induces fine-structure-changing transitions, in the molecular framework, we reparametrize the Born-Oppenheimer potentials to have the form

$$\epsilon_\Omega(R) = \bar{\epsilon}(R) + \delta_\Omega(R), \tag{6}$$

where $\bar{\epsilon}(R)$ is the mean value of $\epsilon_\Lambda(R)$ and $\delta_\Omega(R)$ is the energy defect from it. Inserting this expression into Eq. (3) we obtain

$$\underline{V}(R,\theta,\phi) = \delta_{j,j'}\delta_{\Omega,\Omega'}\bar{\epsilon}(R) + \underline{W}(R,\theta,\phi), \tag{7}$$

where $\underline{W}(R,\theta,\phi)$ has the same form as Eq. (4) except that the term $\epsilon_\Lambda(R)$ is now replaced with δ_Λ. The first term in Eq. (7) is isotropic and diagonal in the fine-structure quantum numbers, but the anisotropic term $\underline{W}(R,\theta,\phi)$ induces fine-structure transitions. The strength of the couplings associated with those transitions is proportional to the defects $\delta_\Lambda(R)$.

In time-independent scattering theory, it is useful to expand the scattering amplitude into a sum of partial waves and express the scattering equations in terms of radial amplitudes. Following the procedure in Ref. [17] we define

$$F_{j\Omega}(\boldsymbol{R}) = \sum_{lm} \sum_{JM} \begin{pmatrix} j & l & J \\ \Omega & m & -M \end{pmatrix} [J]^{1/2} Y_{lm}(\theta\phi) \frac{G_{jl}^{JM}(R)}{R}, \tag{8}$$

where $G_{jl}^{JM}(R)$ is a radial amplitude. According to $3j$ selection rules, the indices J, M in Eq. (8) represent the total angular momentum of the diatom. Inserting Eq. (8) into Eq. (1), we obtain the coupled radial equations [17].

$$\begin{aligned} & \frac{d^2 G_{jl}^{JM}(R)}{dR^2} - \frac{l(l+1)}{R^2} G_{jl}^{JM}(R) - 2\mu \sum_{j'l'} V_{jl}^{j'l'}(R,JM) G_{j'l'}^{JM}(R) \\ & \quad + k_j^2 G_{jl}^{JM}(R) = 0 \end{aligned} \tag{9}$$

for a given J and M. The multichannel radial potential is given by [17]

TABLE I. Itemization of quantum numbers associated with the channel indices for a given value of total angular momentum J. The set of 21 channels can be decomposed into two subsets of different parity. The channel orbital angular momenta l are expressed in terms of J.

Parity $(-1)^J$			Parity $(-1)^{J+1}$		
Channel	l	j	Channel	l	j
1	$J+2$	2	12	$J+1$	2
2	J	2	13	$J-1$	2
3	$J-2$	2	14	$J+3$	3
4	$J+2$	3	15	$J+1$	3
5	J	3	16	$J-1$	3
6	$J-2$	3	17	$J-3$	3
7	$J+4$	4	18	$J+3$	4
8	$J+2$	4	19	$J+1$	4
9	J	4	20	$J-1$	4
10	$J-2$	4	21	$J-3$	4
11	$J-4$	4	-	-	-

$$V_{jl}^{j'l'}(JM,R) = \sum_{\Omega M_S}\sum_{\Lambda}[j,j']^{1/2}[l,l']^{1/2} \times \begin{pmatrix} j & l & J \\ \Omega & 0 & -\Omega \end{pmatrix}\begin{pmatrix} j' & l' & J \\ \Omega & 0 & -\Omega \end{pmatrix} \times \begin{pmatrix} L & S & j' \\ \Lambda & M_S & -\Omega \end{pmatrix} \times \begin{pmatrix} L & S & j \\ \Lambda & M_S & -\Omega \end{pmatrix}\epsilon_\Lambda(R). \quad (10)$$

In this expression anisotropy manifests as nonvanishing couplings among channels of different orbital angular momenta. $V_{jl}^{j'l'}(JM,R)$ couples channels that satisfy angular momentum triangle inequalities as is evident in Table I. If the energy defects among the Born-Oppenheimer potentials ϵ_Λ are ignored, $3j$ symbol closure rules can be applied in Eq. (10), and $V_{jl}^{j'l'}(JM,R)$ reduces to the standard form for an isotropic radial potential, which does not contain couplings between channels of different l and j. From this perspective, anisotropy is a consequence of splittings in the BO energy levels of different Λ.

$V_{jl}^{j'l'}(JM,R)$ is in block-diagonal form with respect to the quantum numbers JM, and it is useful to itemize the channel indices, for given JM, as in Table I. Solving the radial equations and imposing scattering boundary conditions on the asymptotic limit $R\to\infty$ we extract the multichannel radial S matrix $S_{j'l'}^{jl}(JM)$. The scattering amplitude for the system to undergo a transition from electronic state $j'\Omega'$ into $j\Omega$ and for the nuclei to scatter into solid angle $d\mathbf{\Omega}\equiv d\theta\sin\theta d\phi$ following an initial approach defined by angles $\theta_i\phi_i$ is [17]

$$f_{j\Omega}^{j'\Omega'}(\theta\phi;\theta_i\phi_i) = \sum_{lm}\sum_{l'm'}\sum_{JM}[J]\begin{pmatrix} j & l & J \\ \Omega & m & -M \end{pmatrix} \times \begin{pmatrix} j' & l' & J \\ \Omega' & m' & -M \end{pmatrix} \times Y_{lm}(\theta\phi)Y_{l'm'}^*(\theta_i\phi_i)\frac{2\pi i}{k_{j'}^{1/2}k_j^{1/2}}[\delta_{j,j'}\delta_{l,l'} - S_{j'l'}^{jl}(JM)]. \quad (11)$$

The total cross section for Ti to undergo a transition from state $j_b'=j'$ to $j_b=j$ is

$$\sigma(j'\to j) = \frac{v_j}{v_{j'}}\frac{1}{2j'+1}\sum_{\Omega\Omega'}\frac{1}{4\pi}\int d\mathbf{\Omega}\, d\mathbf{\Omega}_i|f_{j\Omega}^{j'\Omega'}(\theta\phi;\theta_i\phi_i)|^2, \quad (12)$$

where $v_{j'},v_j$ are the initial and final velocities of the projectile, respectively. Evaluating Eq. (12) we obtain

$$\sigma(j'\to j) = \frac{\pi}{k_{j'}^2(2j'+1)}\sum_{l,l'}\sum_{J}(2J+1)|T_{j'l'}^{jl}(J)|^2 \quad (13)$$

where

$$T_{j'l'}^{jl}(J) = \delta_{j'l'}^{jl} - S_{j'l'}^{jl}(J)$$

is a radial partial T matrix.

III. RESULTS

In its ground state, titanium has an electronic configuration in which a pair of $3d^2$ electrons are "submerged" [22] in a closed $4s^2$ shell. It is characterized by a ^3F_J term that consists of fine-structure levels $J=4,3,2$ with splittings [23] $E_{J=3}$-$E_{J=2}=1.55\times10^{-3}$Ry and $E_{J=4}$-$E_{J=2}=3.53\times10^{-3}$Ry. In the close approach of Ti with He, the system is described by the BO potentials of the TiHe diatom. They have recently been calculated by Klos *et al.* [22], and in Fig. 1 they are plotted as a function of interatom distance. In that figure, it is evident that the BO energies are nearly degenerate. At the well minimum, the largest energy defect, between the $^3\Sigma$ and $^3\Phi$ states, has the value 0.187 cm^{-1} [22]. In contrast, systems in which the valence electrons are not submerged, such

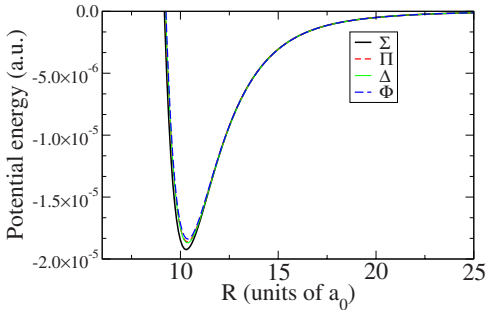

FIG. 1. (Color online) *Ab initio* potential curves for the ground triplet states of the TiHe molecule. The curves are labeled by the electronic BO orbital angular momentum quantum numbers $\Lambda = \Sigma, \Pi, \Delta, \Phi$.

as CHe, OHe, etc., splittings on the order of tens of cm^{-1} [15] are typical.

The suppressed BO energy splittings are a consequence of screening by the outer closed $4s^2$ shell charge density of the inner d-shell electrons [22]. According to the discussion in the previous sections and Eq. (7) the resulting diminished "couplings" δ_i should lead to an inhibition of fine-structure-changing transitions. In Fig. 2 we plot the calculated values for the $j'=3 \rightarrow j=2$ fine-structure-quenching cross sections. For the sake of comparison, we also plot the $j'=3 \rightarrow j=3$ elastic scattering cross sections. The latter are a factor of, at least, 10^4 greater in magnitude than the quenching cross section for the entire energy range considered. At a collision energy $E \approx 0.43$ K, the quenching cross sections exhibit a pronounced local maximum, which is also mirrored in the elastic scattering cross sections. They correspond to a shape resonance for the $l=3$ partial wave. In Fig. 3 we illustrate the behavior of the elastic $l=3$ radial scattering wave functions as the collision energy sweeps through the resonance. Near the resonance energy, the wave function developes a new node and exhibits a rapid variation in its phase shift. Since the collision time delay [24] is proportional to the derivative of the phase shift with respect to energy, transitions are enhanced near the resonance energy. A less pronounced resonance also appears at $E \approx 1.4$K.

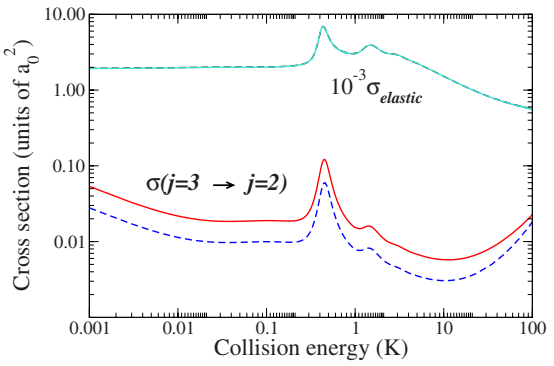

FIG. 2. (Color online) Plot of $j'=3 \rightarrow j=3$ elastic scattering cross sections, multiplied by a factor of 10^{-3}, and the fine-structure-quenching cross sections for the $j'=3 \rightarrow j=2$ transition. Dashed lines represent cross sections obtained using the *ab initio* potentials, whereas the solid lines represent corresponding values obtained using the scaling function introduced in Eq. (15). Collision energies are expressed in units of kelvin.

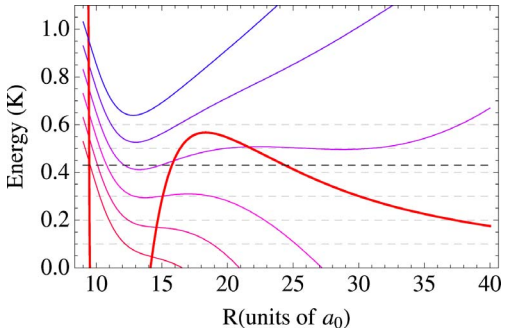

FIG. 3. (Color online) The heavy solid line represents the effective Σ, $l=3$, radial potential as a function of internuclear distance R. The bold dashed line represents the resonance energy at $E \approx 0.43$K. The lighter solid lines represent the elastic scattering radial wave functions (not drawn to scale) for collision energies (shown by the light dashed lines) that sweep through the resonance energy.

In Fig. 4 we plot all three fine-structure-quenching cross sections in this energy range. It is evident from the figure that all cross sections exhibit similar behavior as a function of energy, including the resonance structures. The $3 \rightarrow 2$ transition is the dominant one, presumably because the energy defect between $j=4$ and $j=3$ levels is about 5/3 larger than the $j=3$ to $j=2$ defect. Typically, cross sections for transitions with larger energy defects are smaller.

In Fig. 5 we plot all fine-structure-quenching cross sections for collision energies that correspond to the cryogenic to superthermal temperature range. The cross sections show a steep rise as the collision energy is increased, a consequence of the system sampling the inner repulsive walls of the TiHe BO potentials. In that region, the defects $\delta_i(R)$ become larger, thus leading to enhancement of transition probabilities. At higher collision energies we can ignore the energy defects of the Ti fine-structure levels, and a statistical approach to the collision problem predicts that the cross sections should behave as

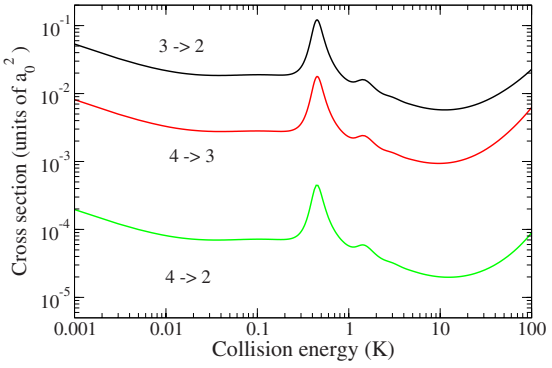

FIG. 4. (Color online) Plot of fine-structure-changing cross sections for low collision energies. Collision energies are expressed in units of kelvin.

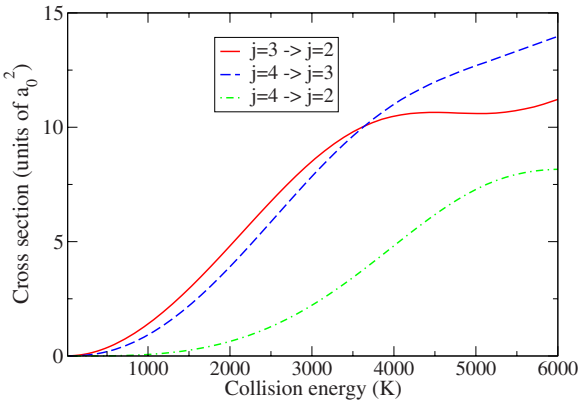

FIG. 5. (Color online) Fine-structure-quenching cross sections at high collision energies.

$$\sigma(j' \to j) \approx \frac{2j+1}{2j'+1}\tilde{\sigma}, \tag{14}$$

where $\tilde{\sigma}$ is an effective mean inelastic cross section. According to Fig. 5, $\frac{\sigma(4\to2)}{\sigma(4\to3)}=0.6$, $\frac{\sigma(4\to2)}{\sigma(3\to2)}=0.7$, and $\frac{\sigma(4\to3)}{\sigma(3\to2)}=1.2$ at $E \approx 6000$K. The corresponding values predicted by Eq. (14) are 0.7, 0.8, and 1.1, respectively, showing good agreement with the former. Using these results we estimate $\tilde{\sigma} \approx 8 \times 10^{-17}$ cm^2 at a collision energy of 6000 K. Though much larger than our calculated cross sections at cryogenic temperatures, $\tilde{\sigma}$ is still smaller than typical [5] fine-structure-changing cross sections at higher energies. In Table II we tabulate the fine-structure-quenching rate coefficients for a large temperature range. Suppression is clearly evident for temperatures up to $T \approx 100$ K. In studies of fine-structure transitions of C(^3P) and Si(^3P) in collisions with He [9], rates on the order of 10^{-11}cm^{3}s^{-1} were reported for the temperature range $100 < T < 390$K. In contrast, according to Table II, only at room temperature do the rates approach the 10^{-12} cm^2 s^{-1} figure.

Recent experiments by Lu *et al.* [19] measured the fine-structure-changing rate coefficients

$$k(j' \to j) \equiv \langle v\sigma(j' \to j) \rangle$$

where the $\langle\ \rangle$ notation implies thermal averaging over collision velocities v, for the TiHe system at cryogenic temperatures. The results of those measurements are presented in Fig. 6 along with the values obtained in our theoretical calculations. The dashed line in that figure is the calculated rate using the *ab initio* potential curves given by Klos *et al.* [22] and shown in Fig. 1. The calculated rates are in reasonable agreement with the measurements, exhibiting a similar energy dependence. However, the former values are somewhat smaller in magnitude when compared to those obtained by the laboratory measurements. In a study of the Zeeman relaxation rate of Ti, in a strong magnetic field, by collisions with He, Hancox *et al.* [15] found that use of the *ab initio* BO potentials failed to predict the precise measured values. However, by a rescaling of the *ab initio* potentials, they were able to calculate rates that are in harmony with experiment. In Table I of that paper they provide "experimental" values for the difference in binding energies, ΔD, between the ground electronic states of the TiHe molecule. They are given by $\Delta D_{\Sigma\text{-}\Pi}=0.056$, $\Delta D_{\Sigma\text{-}\Delta}=0.049$, and $\Delta D_{\Sigma\text{-}\Phi}=0.077$ expressed in units of cm^{-1}. They differ from the *ab initio* values $\Delta D_{\Sigma\text{-}\Pi}=0.138$, $\Delta D_{\Sigma\text{-}\Delta}=0.120$, and $\Delta D_{\Sigma\text{-}\Phi}=0.187$, respectively. Though an explicit form for the rescaled potentials was not given in [15], here we rescale each $\epsilon_\Pi(R), \epsilon_\Delta(R), \epsilon_\Phi(R)$ BO curve by a constant factor in order to reproduce the binding energies given in Ref. [15]. Using the rescaled potentials we calculated $k(3\to2)$ and plotted those values by the dash-dotted line in Fig. 6. Indeed, the resulting rates seem to be in better agreement with experiment, though they do not fall within the experimental error bars. In our calculations we found that the $\sigma(3\to2)$ cross sections are very sensitive to the value of the BO potentials near the inner repulsive wall. We therefore consider an alternative rescaling of the BO potentials from that given in Ref. [15]. We introduce the scaling function

$$w(R) = 1.0 + \frac{a}{1+\exp\left(\frac{(R-R_0)^2}{d}\right)} \tag{15}$$

TABLE II. Fine-structure-quenching rate coefficients, expressed in units of cm^3 s^{-1}. Temperature is expressed in kelvin.

T (K)	$k(3\to2)$	$k(4\to3)$	$k(4\to2)$
5	3.53×10^{-15}	5.67×10^{-16}	1.25×10^{-17}
10	4.91×10^{-15}	8.78×10^{-16}	1.68×10^{-17}
20	9.77×10^{-15}	2.15×10^{-15}	3.48×10^{-17}
40	2.87×10^{-14}	8.57×10^{-15}	1.4×10^{-16}
60	6.44×10^{-14}	2.33×10^{-14}	4.58×10^{-16}
100	2.02×10^{-13}	9.13×10^{-14}	2.7×10^{-15}
140	4.47×10^{-13}	2.3×10^{-13}	9.5×10^{-15}
180	8.13×10^{-13}	4.57×10^{-13}	2.47×10^{-14}
220	1.31×10^{-12}	7.88×10^{-13}	5.29×10^{-14}
300	2.71×10^{-12}	1.8×10^{-12}	1.7×10^{-13}

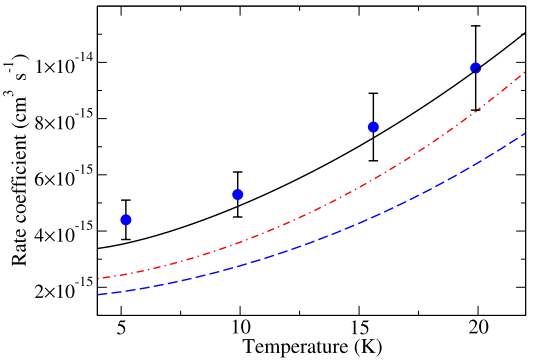

FIG. 6. (Color online) Fine-structure-quenching rate coefficients. Dashed line represents theoretical predictions based on *ab initio* potential curves calculated in Ref. [22]. The dash-dotted line represents the results of the calculation using the scaled potentials suggested in Ref. [15]. Solid line represents the calculated collision data obtained using the rescaled potentials discussed in this paper. Plotted points, measured values.

with adjustable parameters a, R_0, and d, and we multiply all BO potentials by this common factor. With the choice $a=-0.6$, $R_0=9.0$, and $d=0.3$, we employ the resulting potentials to calculate $k(3\rightarrow 2)$. The results are plotted by the solid line shown in Fig. 6. The calculated rates are in excellent agreement with the measured rates at higher temperatures. At $T=5.2$K the calculated rate is in fair agreement with the experimental value, just missing the lower error bar. Because the contribution from the resonance, shown in Fig. 2, to the lower-energy rate coefficients is significant, a more accurate description of the BO potentials, which predicts the exact location of the resonance, is needed. Additional measurements at $T\approx 0.5$K will help facilitate such a program. The advantage of the scaling suggested by Eq. (15) is that, with the choice of parameters given above, it modifies the *ab initio* potentials only in the inner region of the repulsive wall in a localized region near $R=9a_0$. The scaling leads to an insignificant change in the binding energies predicted by the *ab initio* calculations, as well as the value of the potentials in the regions of R to the right of the minimum and in the asymptotic region. In Fig. 2 we also plot $\sigma(3\rightarrow 2)$ as well as the elastic cross sections obtained using our scaled potentials. The effect of the rescaling on the elastic cross sections is hardly perceptible in that figure; however, it has a pronounced effect on the values of the fine-structure-changing cross section, even toward the ultracold limit. The data illustrated in Figs. 4 and 5, as well as the rate coefficients tabulated in Table II, were generated using the rescaled potentials described above.

IV. DISCUSSION AND CONCLUSION

We presented FS changing cross sections and rate coefficients for the Ti-He system for collision energies corresponding to temperatures that span the millikelvin to superthermal range. Our calculations show that the resulting cross sections are significantly suppressed over a wide collision energy range. Our investigations indicate that the mechanism proposed by Doyle [13] to explain suppression effects in relaxation of Zeeman split m levels is also responsible for suppression of J-changing transitions. Our calculations suggest that the effect may persist into the thermal collision energy range. We found that the use of the *ab initio* Ti-He potentials of Klos *et al.* [22] in our calculations gave reasonable agreement with the results of the laboratory measurements [19] for the $j=3\rightarrow 2$ rate coefficients in the 5–20 K temperature interval. In order to bring the theoretical rates into better agreement with the experimental results, we proposed a slight modification, in terms of a simple scaling function, of the *ab initio* potentials. We found that FS quenching rates are sensitive to the value of the BO energies in the region of the inner repulsive wall. Our rescaling is significant only in that region and results in a less than 1% change in the value of the BO binding energies. This conclusion differs from that given in Ref. [15], in which it was argued that the m-changing quenching rates are sensitive to the details of the BO potentials in the region to the right, and at larger interatomic separations, of the BO potential minimum. Their rescaling leads to significant differences from the *ab initio* values in the BO binding energies.

ACKNOWLEDGMENTS

We thank Jacek Kłos for providing the Ti-He molecular potentials. B.Z. was supported, in part, by the Department of Energy under Grant No. DE-FG36-05GO85028.

APPENDIX

In the study of Zeeman relaxation by m-changing transitions in Ref. [14], Krems *et al.* employ an effective interaction that has the form

$$\tilde{V}=\sum_k \tilde{V}_k(R)P_k(\boldsymbol{r}\cdot\boldsymbol{R})=\sum_k \tilde{V}_k(R)\sum_m \frac{4\pi}{2k+1}Y^*_{km}(\hat{\boldsymbol{r}})Y_{km}(\theta\phi), \tag{A1}$$

where $\boldsymbol{r}$ are the electronic coordinates and $\boldsymbol{R}$ is the interatom separation vector [25]. P_k is a Legendre polynomial of order k, and $\tilde{V}_k(R)$ is an effective radial potential [14]. A similar expansion was employed [4] in a study of fine-structure excitation, via long-range interactions, of hydrogenic ions by collisions with protons. Below we demonstrate that Eq. (4), the interaction potential that drives J-changing transitions, is equivalent to an expression that is obtained when taking matrix elements of expansion (A1) with respect to the asymptotic basis states $|j\Omega\rangle$.

The interaction potential given by Eq. (4) can be expanded by the complete set of functions on the two-sphere, the spherical harmonics. Thus

$$V(R,\theta,\phi)=\sum_{km} c_{km}(R)Y_{km}(\theta,\phi), \tag{A2}$$

where the expansion coefficients $c_{km}(R)$ are obtained by equating this expression with Eq. (4) and projecting out the spherical harmonics. In carrying out this program, using Eq. (73) in Ref. [17], we obtain

$$c_{km}(R)=\sum_{\Lambda M_S}\sum_{\Omega_1}\sqrt{4\pi[k,j,j']}(-1)^{\Omega_1+\Omega'}\times\begin{pmatrix}k & j & j'\\ m & \Omega & -\Omega'\end{pmatrix}\begin{pmatrix}k & j & j'\\ 0 & \Omega_1 & -\Omega_1\end{pmatrix}\times\begin{pmatrix}L & S & j\\ \Lambda & M_S & -\Omega_1\end{pmatrix}\begin{pmatrix}L & S & j'\\ \Lambda & M_S & -\Omega_1\end{pmatrix}\epsilon_\Lambda(R). \tag{A3}$$

We introduce a spherical tensor $\boldsymbol{T}^{(k)}_m$ of rank k in the asymptotic product space $|LM\rangle\otimes|SM_S\rangle$ for $L=3$ and $S=1$ and which is spanned by $|j\Omega\rangle\equiv|j\Omega(LS)\rangle$ [17]. Thus, according to the Wigner-Eckart theorem,

$$c_{km}(R)=\langle j\Omega|\boldsymbol{T}^{(k)}_m|j'\Omega'\rangle, \tag{A4}$$

provided that the reduced matrix element,

$$\langle j||\boldsymbol{T}^{(k)}||j'\rangle = \sum_{\Lambda M_S}\sum_{\Omega_1}\sqrt{4\pi[k,j,j']} \times(-1)^{\Omega_1+\Omega'+\Omega+j}\begin{pmatrix} k & j & j' \\ 0 & \Omega_1 & -\Omega_1 \end{pmatrix} \times\begin{pmatrix} L & S & j \\ \Lambda & M_S & -\Omega_1 \end{pmatrix}\begin{pmatrix} L & S & j' \\ \Lambda & M_S & -\Omega_1 \end{pmatrix}\epsilon_\Lambda(R). \tag{A5}$$

Now $V^{j\Omega}_{j'\Omega'}(\theta,\phi,R)$ can be expressed as matrix elements of the scalar product of spherical tensor operators of rank k, i.e.,

$$V^{j\Omega}_{j'\Omega'}(\theta,\phi,R) = \langle j\Omega|\boldsymbol{V}^0|j'\Omega'\rangle,$$

$$\boldsymbol{V}^{(0)} \equiv \sum_k \boldsymbol{Y}^{(k)}(\theta\phi)\cdot\boldsymbol{T}^{(k)} = \sum_k\sum_q (-1)^q Y_{kq}(\theta\phi)T^{(k)}_{-q}. \tag{A6}$$

In the same manner Eq. (A1) can be expressed as

$$\tilde{V} = \tilde{\boldsymbol{V}}^{(0)} \equiv \sum_k \boldsymbol{Y}^{(k)}(\theta\phi)\cdot\tilde{\boldsymbol{T}}^{(k)} \tag{A7}$$

where

$$\tilde{\boldsymbol{T}}^{(k)} = \boldsymbol{Y}^{(k)}(\hat{\boldsymbol{r}})\otimes \boldsymbol{I}V_k(R) \tag{A8}$$

is a direct product in $|LM\rangle\otimes|SM_S\rangle$ space, and $\boldsymbol{I}$ is the identity operator in spin space. Taking the matrix elements of Eq. (A1) with respect to the asymptotic states $|j\Omega\rangle$, we obtain

$$\langle j\Omega|\tilde{V}(R)|j'\Omega'\rangle = \sum_k \boldsymbol{Y}^{(k)}(\theta\phi)\cdot\langle j\Omega|\tilde{\mathbf{T}}^{(k)}|j'\Omega'\rangle. \tag{A9}$$

The reduced matrix element can be evaluated [26], to give

$$\langle j||\tilde{\boldsymbol{T}}^{(k)}||j'\rangle = \tilde{V}_k(R)\sqrt{\frac{4[j,j']\pi}{[k]}}[L](-1)^{S+j'+k} \times\begin{pmatrix} L & k & L \\ 0 & 0 & 0 \end{pmatrix}\begin{Bmatrix} L & j & S \\ j' & L & k \end{Bmatrix}. \tag{A10}$$

According to Aquilanti and Grossi [27] the multipole moments $\tilde{V}_k(R)$ can be expressed in terms of the BO eigenvalues ϵ_Λ by the relation

$$\begin{pmatrix} L & k & L \\ 0 & 0 & 0 \end{pmatrix}\tilde{V}_k(R) = \sum_\Lambda \frac{[k]}{[L]}(-1)^\Lambda\begin{pmatrix} L & k & L \\ \Lambda & 0 & -\Lambda \end{pmatrix}\epsilon_\Lambda(R). \tag{A11}$$

Inserting Eq. (A11) into Eq. (A10) we obtain

$$\langle j||\tilde{\mathbf{T}}^{(k)}||j'\rangle = \sum_\Lambda \sqrt{4\pi[k,j,j']}(-1)^{S+j'+k+\Lambda} \times\begin{pmatrix} L & k & L \\ \Lambda & 0 & -\Lambda \end{pmatrix}\begin{Bmatrix} L & j & S \\ j' & L & k \end{Bmatrix}\epsilon_\Lambda(R). \tag{A12}$$

Using the identity [26]

$$\sum_{M_S}(-1)^{j+M_S}\begin{pmatrix} k & j & j' \\ 0 & \Omega_1 & -\Omega_1 \end{pmatrix} \times\begin{pmatrix} L & S & j \\ \Lambda & M_S & -\Omega_1 \end{pmatrix}\begin{pmatrix} L & S & j' \\ \Lambda & M_S & -\Omega_1 \end{pmatrix} = (-1)^{S+j'}\begin{pmatrix} L & k & L \\ \Lambda & 0 & -\Lambda \end{pmatrix}\begin{Bmatrix} L & j & S \\ j' & L & k \end{Bmatrix} \tag{A13}$$

and comparing expressions (A12) and (A5), we find

$$\langle j||\boldsymbol{T}^k||j'\rangle = \langle j||\tilde{\boldsymbol{T}}^k||j'\rangle, \tag{A14}$$

and this, according to Eqs. (A6) and (A7), proves our assertion.

[1] A. Dalgarno and R. McCray, Annu. Rev. Astron. Astrophys. **10**, 375 (1972).
[2] D. R. Bates, Proc. Phys. Soc. London, Sect. B **64**, 805 (1951).
[3] R. D. Sharma, B. Zygelman, F. von Esse, and A. Dalgarno, Geophys. Res. Lett. **21**, 1731 (1994).
[4] B. Zygelman and A. Dalgarno, Phys. Rev. A **35**, 4085 (1987).
[5] R. H. G. Reid and A. Dalgarno, Phys. Rev. Lett. **22**, 1029 (1969).
[6] F. H. Mies, Phys. Rev. A **7**, 942 (1973).
[7] J. M. Launay and E. Roueff, J. Phys. B **10**, 879 (1977).
[8] S. D. Le Picard, B. Bussery-Honvault, C. Rebrion-Rowe, P. Honvault, A. Canosa, J. M. Launay, and B. R. Rowe, J. Chem. Phys. **108**, 10319 (1998).
[9] S. D. Le Picard, P. Honvault, B. Bussery-Honvault, A. Canosa, S. Laube, J.-M. Launay, B. Rowe, D. Chastaing, and I. R. Sims, J. Chem. Phys. **117**, 10109 (2002).
[10] V. Kokoouline, R. Santra, and C. H. Greene, Phys. Rev. Lett. **90**, 253201 (2003).
[11] A. Derevianko, S. G. Porsev, S. Kotochigova, E. Tiesinga, and P. S. Julienne, Phys. Rev. Lett. **90**, 063002 (2003).
[12] D. Hansen and A. Hemmerich, Phys. Rev. Lett. **96**, 073003 (2006).
[13] C. I. Hancox, S. C. Doret, M. T. Hummon, L. Luo, and J. Doyle, Nature (London) **431**, 281 (2004).
[14] R. V. Krems, J. Kłos, M. F. Rode, M. M. Szczesniak, G. Chałasinski, and A. Dalgarno, Phys. Rev. Lett. **94**, 013202 (2005).
[15] C. I. Hancox, S. C. Doret, M. T. Hummon, R. V. Krems, and J. M. Doyle, Phys. Rev. Lett. **94**, 013201 (2005).
[16] A. A. Buchachenko, G. Chałasinski, M. M. Szczesniak, and R. V. Krems, Phys. Rev. A **74**, 022705 (2006).
[17] B. Zygelman, A. Dalgarno, and R. D. Sharma, Phys. Rev. A **49**, 2587 (1994).
[18] R. deCarvalho, J. M. Doyle, B. Friedrich, T. Guillet, J. Kim, D. Patterson, and J. D. Weinstein, Eur. Phys. J. D **7**, 289 (1999).
[19] M.-J. Lu, K. S. Hardman, J. Weinstein, and B. Zygelman, Phys. Rev. A **77**, 060701(R) (2008).
[20] T. Yildirim and S. Ciraci, Phys. Rev. Lett. **94**, 175501 (2005).
[21] B. Zygelman, A. Dalgarno, and R. D. Sharma, Phys. Rev. A

50, 3920 (1994).
[22] J. Klos, M. Rode, J. Rode, G. Chalasinski, and M. Szczesniak, Eur. Phys. J. D **31**, 429 (2004).
[23] Y. Ralchenko, F.-C. Jou, D. Kelleher, A. Kramida, A. Musgrove, J. Reader, W. Wiese, and K. Olsen, *NIST Atomic Spectra Database*, 3rd ed. (National Institute of Standards and Technology, Washington, DC, 2007), http://physics.nist.gov/asd3
[24] J. R. Taylor, *Scattering Theory: The Quantum Theory of Nonrelativistic Collisions* (Dover, New York, 2006).
[25] R. V. Krems, G. C. Groenenboom, and A. Dalgarno, J. Phys. Chem. A **108**, 8941 (2004).
[26] A. de Shalit and I. Talmi, *Nuclear Shell Theory* (Academic, New York, 1963).
[27] V. Aquilanti and G. Grossi, J. Chem. Phys. **73**, 1165 (1980).